Electric Power Systems Research 200 (2021) 107466

Contents lists available at ScienceDirect

Electric Power Systems Research

journal homepage: www.elsevier.com/locate/epsr

Analysis of the resonance phenomenon in unmatched power cables with the resonance surface response

Tamiris G. Bade [*,a], James Roudet [a], Jean-Michel Guichon [a], Patrick Kuo-Peng [b], Carlos A. F. Sartori [c,d]

[a] Univ. Grenoble Alpes, CNRS, Grenoble INP, G2Elab, 21 av des martyrs, Grenoble 38000, France
[b] Federal University of Santa Catarina, GRUCAD, campus Trindade, Florianópolis 88040-970, Brazil
[c] Escola Politécnica da Universidade de São Paulo (PEA/EPUSP), São Paulo, SP 05508-010, Brazil
[d] Instituto de Pesquisas Energéticas e Nucleares (IPEN/CNEN-SP), São Paulo, SP 05508-900, Brazil

ARTICLE INFO

Keywords:
Power cable
Resonance
Switching harmonics
Power converters
Electromagnetic compatibility

ABSTRACT

Power converters are an essential part of modern power systems, giving flexibility to the power transportation and allowing the insertion of a wide range of different energy sources. One drawback of the converters is that the supraharmonic conducted emissions introduced by them can compromise the stability of these systems through electromagnetic interference (EMI). Electromagnetic compatibility (EMC) filters are used to prevent such problems. Nevertheless, these filters are designed to respect standards based on measurements in conditions considerably different from real applications. Particularly, if a converter is connected to electrically long cables its conducted emissions may be amplified by the resonance phenomenon. The method described in this paper allows the definition of a range for the filters input impedances where the conducted emissions in a long cable will not be amplified beyond established levels. In some cases the method allows the visualization of three-dimensional surfaces indicating the magnitude, frequency and position of the resonance phenomenon. In the general case these surfaces are defined on higher dimensions and can be analyzed with deterministic optimization algorithms. The originality of this paper resides in the generalized analysis of the resonance phenomenon, that it is based on frequency-dependent cable parameters and applies to unbalanced systems.

1. Introduction

Power converters insertion in modern power systems has increased considerably in recent years, and tends to continue increasing with the investments towards smart grids, renewable energy sources, and high voltage DC lines, to cite a few applications. One drawback of the converters is the increase of the total harmonic distortion (THD), for low frequencies, and electromagnetic interference (EMI) for the supra-harmonic frequency band [1]. The filters responsible for attenuating the switching harmonics generated by the converters are usually designed for the test conditions, without taking into account the behavior of the system as a whole. Moreover, designers often choose to reduce or remove output filters on power converters that are connected to inductive loads, such as induction motors [2]. To guarantee the robustness of the system these filters must be adapted to the possibility of resonance-due overvoltages and overcurrents.

The conducted emissions may be amplified by the resonance phenomenon if they flow through an electrically long cable. Some examples of applications where the resonance of switching harmonics may cause damage to the installation are: the connections between offshore power plants and onshore substations [3,4]; in electric transportation applications such as trains (catenary lines) [5], electric vehicles [6] or electric aircraft [7]; and on long power cables connecting AC motors to their drives [2,8–11]. The aforementioned papers mention resonance-linked EMI problems originating from overvoltages and poor power quality, which may lead to dysfunctions of sensitive devices, tripping of circuit breakers and even systems outages.

With the advent of wide-band gap semiconductors the resonance tends to appear in shorter cables, because with faster switching times the frequencies of the harmonics introduced in the system tend to rise. Therefore, an effective design method able to improve the robustness of a system facing resonance tends to become more relevant.

The difficulties of an accurate model of the resonance phenomenon arise from the frequency-dependent behavior of the power cables used in

* Corresponding author.
E-mail address: tamiris.grossl-bade@g2elab.grenoble-inp.fr (T.G. Bade).

https://doi.org/10.1016/j.epsr.2021.107466
Received 27 January 2021; Received in revised form 5 June 2021; Accepted 11 July 2021
Available online 24 July 2021

these applications [12]. Indeed, the resonance frequency of a cable is not constant when its per-unit-length (p.u.l.) parameters are frequency dependent [13]. To determine the resonance frequency of such cables a numerical solution is necessary [14,15]. Most of the papers in the literature use a simplified cable model with constant p.u.l. transmission-line parameters [2–11], and constant parameters models might lack in accuracy to represent the resonance behavior in a long cable. Some applications, such as damping the resonance-due amplification with notch filters [4], could considerably benefit from the accuracy of a frequency-dependent cable model.

The impact of the frequency-dependency of the cable parameters on the resonance is emphasized in [14], where a method to calculate the resonance frequency for transmission lines connected to resistive loads is given. However, this method cannot be applied to reactive loads. Nevertheless, in electric systems reactive loads are frequent where device with input and/or output filters are present, for instance [2,4]. Therefore, the generic resonance prediction model proposed here is a relevant contribution.

This paper describes an innovative analysis and representation method denominated the “resonance surface response”. It describes the behavior of the resonance phenomenon in a given multiconductor transmission line in function of the impedances connected to its terminals. The linearization of power converters [16] is required when such devices are connected to the cable. The proposed analysis gives a more general description of the resonance behavior than those presented in the literature, giving the resonance frequency, position and amplification for a generic linear system with any number of conductors in the line. It is based in frequency-dependent p.u.l. parameters and can be applied to any cable connected to any linear load, even if it is unbalanced.

A former paper from the same authors gives an example of the applicability of the method proposed here [17]. This previous paper is limited to the analysis of three-conductor balanced systems, where the resonance surfaces are represented on no more than three dimensions.

In this paper the analysis of asymmetric multiconductor systems with the resonance surface response is described in firsthand, what leads to the analysis of a higher dimensional surface with an optimization algorithm. Also, a few analyses derived from the surface method are first introduced in this work: the impact of cable length on the resonance amplification and the comparison of the resonance behavior between different types of cable. Particularly, it is demonstrated that this method is efficient when the cable parameters used in the model are frequency-dependent.

The analysis proposed here is performed for a frequency band from hundreds of *kHz* to tens of *MHz*, and can be particularly useful in the design of robust EMC filters. As aforementioned, the model requires a linearization of the power converters originating the perturbations. For an EMI study such as the one proposed in this paper a linear model in the supraharmonic frequency band is convenient, and some examples can be found in [16,18].

However, the method can be easily adapted to other frequency bands. The only limitation of the model arises from the validity of the equivalent linear model chosen for the power converters. Indeed, there are some cases of dangerous resonance phenomenon in low frequencies such as large-scale distributed power plants [19,20] and offshore power plants [21], for which a transfer function model of the converter would be more convenient.

The resonance surface response method is described in Section 2. A first example of a two-conductor transmission line leading to three-dimensional resonance surface responses is shown in Section 3, and an example with a three-conductor transmission line leading to seven-dimension surfaces is detailed in Section 4.

2. The resonance in transmission lines

The resonance phenomenon may occur in transmission lines (TL) as in many other physical systems: if the line impedances are not matched, the voltage and current waves traveling through the line are reflected at its terminals and, at specific frequencies, their superposition leads to an amplification of the exciting wave.

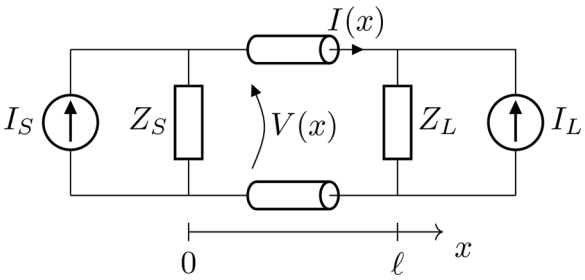

Fig. 1. Schematics of a generic two-conductor cable system, Norton equivalents at the terminals.

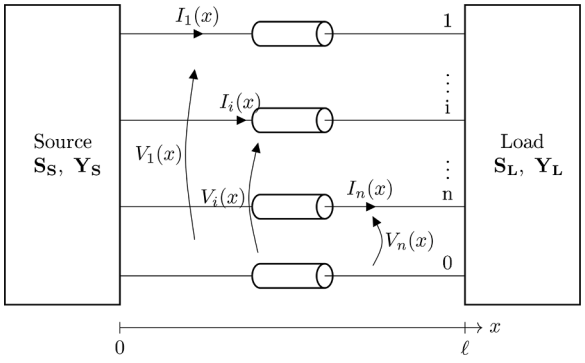

Fig. 2. Generic system with multiconductor cable, devices or network connected to the cable terminals represented by Thévénin/Norton $n+1$-port equivalent circuits.

A generic two-conductor system is represented in Fig. 1. Its reflection coefficients are given by Eqs. (1) and (2), and the condition of matched impedances is given in (3). In these equations, Z_c is the characteristic impedance of the line.

$$\Gamma_L = \frac{Z_L - Z_c}{Z_L + Z_c} \tag{1}$$

$$\Gamma_S = \frac{Z_S - Z_c}{Z_S + Z_c} \tag{2}$$

$$Z_L = Z_S = Z_c \tag{3}$$

In power electronics applications the input or output impedance of the devices are not likely to be matched with the characteristic impedance of the cables. That leads to the presence of medium frequency harmonics due to the switched current and voltage in the converter. If some of these harmonics match the natural frequencies of the cable, they might be amplified by the resonance phenomenon.

The natural frequencies of a TL can be found by minimizing its input impedance (4) [13]. Finding these minima analytically is complicated: the variables Z_S, Z_L, Z_c and γ are frequency dependent, what makes the derivative of (4) in relation to the frequency cumbersome.

$$Z(0) = Z_S \,//\, Z_c \frac{Z_L + Z_c \tanh(\ell\gamma)}{Z_c + Z_L \tanh(\ell\gamma)} \tag{4}$$

More specifically, the variations of γ with the frequency gives a frequency dependent propagation speed v, what demands a numerical solution for the resonance frequency even if the other variables were real constants, as shown in [14]. The aforecited paper gives a numerical method to determine the resonance frequency for $Z_S \to \infty$ and for a

resistive load $Z_L = R$, but not for a generic system.

The generic system under study is represented in Fig. 2, consisting of a multiconductor cable connected to linear loads. The analysis of the resonance phenomenon proposed in this paper consists on:

- Fixing the input voltage of the line $\mathbf{V}(0)$ with voltage sources of constant amplitude and variable frequency;
- Simulating the voltages along the line in a frequency-sweep analysis;
- Storing the highest values of voltage obtained from the simulation results.

The highest values of voltages stored will compose the set of data hereafter denominated the "resonance surface response".

The simulations are performed with an analytic frequency-domain simulator described and experimentally validated in [12]. The simulator is based on the numerical solution for $V(x)$ and $I(x)$ of Eqs. (5) to (11) [22], which are an analytical solution to model the $n+1$-conductor cable connected to generic multiport linear systems as illustrated in Fig. 2.

$$\begin{bmatrix} \mathbf{V}(x) \\ \mathbf{I}(x) \end{bmatrix} = \begin{bmatrix} \mathbf{\Phi}_1(x) & \mathbf{\Phi}_2(x) \\ \mathbf{\Phi}_3(x) & \mathbf{\Phi}_4(x) \end{bmatrix} \begin{bmatrix} \mathbf{V}(0) \\ \mathbf{I}(0) \end{bmatrix} \tag{5}$$

$$\mathbf{\Phi}_1(x) = \mathbf{Z}_c \cosh\left(x\sqrt{\mathbf{YZ}}\right)\mathbf{Y}_c \tag{6}$$

$$\mathbf{\Phi}_2(x) = -\mathbf{Z}_c \sinh\left(x\sqrt{\mathbf{YZ}}\right) \tag{7}$$

$$\mathbf{\Phi}_3(x) = -\sinh\left(x\sqrt{\mathbf{YZ}}\right)\mathbf{Y}_c \tag{8}$$

$$\mathbf{\Phi}_4(x) = \cosh\left(x\sqrt{\mathbf{YZ}}\right) \tag{9}$$

$$\mathbf{I}(0) = \mathbf{I}_S - \mathbf{Y}_S\mathbf{V}(0) \tag{10}$$

$$-\mathbf{I}(\ell) = \mathbf{I}_L - \mathbf{Y}_L\mathbf{V}(\ell) \tag{11}$$

In Eqs. (5) to (9), x is the space axis parallel to the line, ℓ is the cable length, $\mathbf{I}$ and $\mathbf{V}$ are vectors of size n containing respectively the currents of each active conductor and the voltages relative to the reference conductor; $\mathbf{Z}_c = \mathbf{Y}^{-1}\sqrt{\mathbf{YZ}}$ is the characteristic impedance matrix,$\mathbf{Y}_c = \mathbf{Z}_c^{-1}$ is the characteristic admittance matrix and $\sqrt{\mathbf{YZ}}$ is the non-diagonalized propagation matrix. Matrices $\mathbf{Z} = \mathbf{R} + j\omega\mathbf{L}$ and $\mathbf{Y} = \mathbf{G} + j\omega\mathbf{C}$ are the p.u.l. impedance and admittance matrices, respectively. The definition of the p.u.l. resistance $\mathbf{R}$, inductance $\mathbf{L}$, conductance $\mathbf{G}$ and capacitance $\mathbf{C}$ matrices can be found in [22]; j is the imaginary unity and ω is the angular frequency. In Eqs. (10) and (11) $\mathbf{Y}_S$ and $\mathbf{Y}_L$ are the input admittance matrices and $\mathbf{I}_S$ and $\mathbf{I}_L$ are vectors of current sources of a $n+1$-port Norton equivalent circuit as described in [23].

As the simulations are performed in function of the frequency, no approximations are needed to represent the frequency-dependency of the cable parameters. Instead, the parameters identified from input impedance measurements are used in the simulator. In this paper the parameter matrices $\mathbf{Z}$ and $\mathbf{Y}$ for each of the cables were experimentally identified as described in [12,24].

Moreover, because the equations are written in function of the physical reference for voltages and currents instead of a modal reference, there are no limitations on the structure of the devices connected to the cable terminals. The only requirement is that the device or network connected to the cable has a linear equivalent model, e.g. Norton or Thévénin equivalents.

The resonance surface responses obtained from this model are described in the following sections, a three-dimensional example is given in section 3.

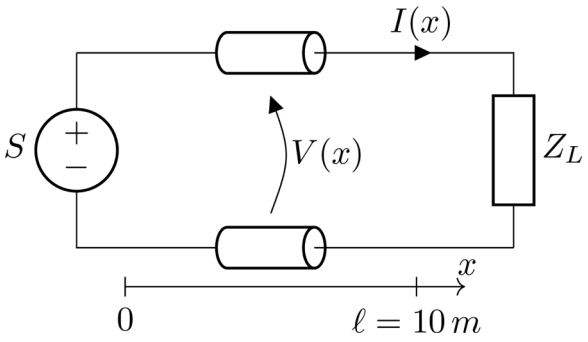

Fig. 3. Schematics of the two-conductor cable system under study, voltage source $S = 1V$ with variable frequency, cable length $\ell = 10\,m$. Resonance analysis performed in function of $Z_L = A + jB$.

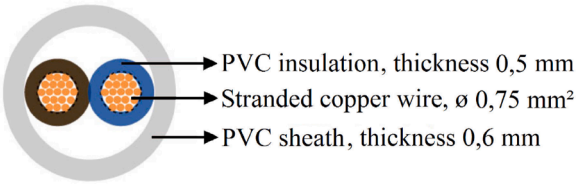

Fig. 4. Cross-section of the two-conductor $0.75\,mm^2$ cable.

Table 1
Range of values used in the numerical analysis leading to the resonance surface response, cable length $\ell = 10\,m$.

Variable	Range	Number of points	Scale
A	$[10^{-2}, 10^{5}]\ \Omega$	402	log
B	$[-10^{5}, -10^{-2}] \cup [10^{-2}, 10^{5}]\ \Omega$	402	log
f	[0.1, 10] MHz	5000	log
x	$[0, \ell]$ m	21	linear

3. Three-dimensional resonance surface response

In this section a three-dimensional resonance surface response example will be presented. The surface is plotted in function of two variables: the real and imaginary parts of the load impedance. The third dimension is used to present the results (voltage, frequency or position of the resonance). This limitation forces the simplification of the generic system in Fig. 2 to the system shown in Fig. 3, which was adopted for this analysis.

The current source in the general model was converted to a voltage source S for convenience, and the resonance surface response is plotted in function of the voltage $V(x)$ for an input voltage $S = 1\,V$.

The cable parameters are those of a two-conductor cable of section $0.75\,\text{mm}^2$ commonly used for power cords of low power devices. Its cross-section is presented in Fig. 4. They were identified from input impedance measurements and can be found in Fig. 2.30 of [24].

The resonance surface response is calculated by evaluating the voltage envelope along the 10 m long cable for all the combinations of the variables in Table 1. The maximal voltage obtained for each impedance $Z_L = A + jB$ is stored, along with the frequency and position where it takes place. The simulations are performed with the frequency-domain simulator described and validated experimentally in [12].

The surfaces composing the resonance surface response are plotted in Fig. 5. The maximal voltages obtained for each pair (A, B) is plotted in Fig. 5c and d. The resonance frequency to which these maxima occur is plotted in Fig. 5c and d. The position along the cable where the maxima take place is plotted in Fig. 5e and f. The figures are split in two to represent positive and negative values of B in log scale.

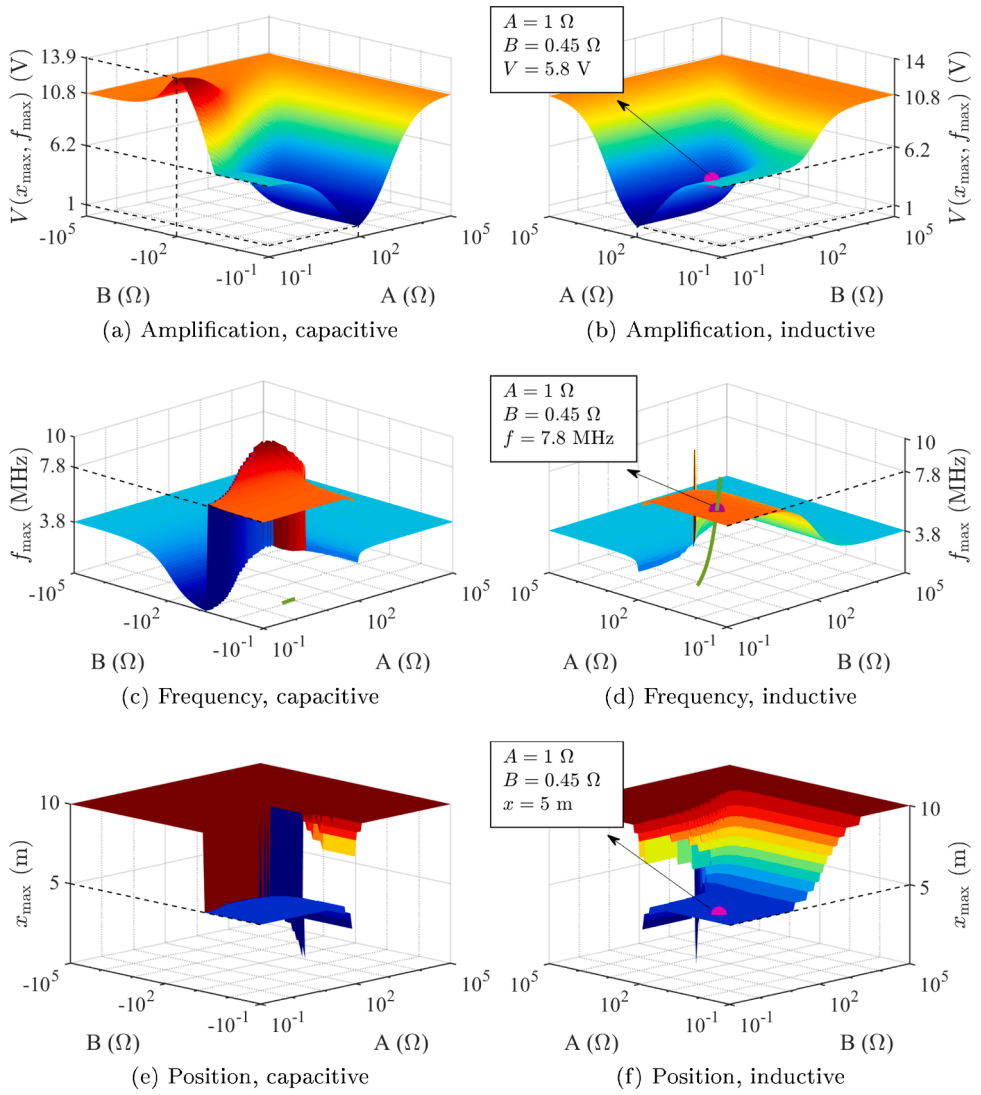

Fig. 5. Resonance Surface Response for $0,75mm^2$ two-conductor cable of length $\ell = 10\,m$ with $V(0) = 1\,V$, propagation speed $v \approx 1.54 \times 10^8\,m\,/s$; Green line: impedance Z_{L_e}, pink markers: intersections with Z_{L_e}.

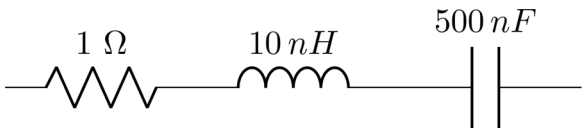

Fig. 6. Z_{L_e}: Example of load for the intersection with the resonance surface response, a low impedance was chosen to enable an easy reading of Fig. 5d.

The labeled points in Fig. 5 correspond to the intersection between the surfaces and the impedance of an example load Z_{L_e}. The load is given in Fig. 6 and will be used later in this section as an example of how the resonance surface response can be exploited.

Note that the frequency and voltage amplification surfaces are mirrored: the higher is the voltage amplification the lower is the resonance frequency corresponding to it, since the cable losses are smaller for lower frequencies.

The resonance surface response presents three zones corresponding to the well-known behavior of the resonance phenomenon (propagation speed in the cable $v \approx 1.54 \times 10^8\,m/s$):

- The zone with high values of A or B: approaches the open-ended cable, resonance frequency of $f_r = v/4\ell$ taking place at $x = \ell$ with high voltage amplification;
- The zone with low values of A and B: approaches the short-circuited cable, resonance frequency of $f_r = v/2\ell$ taking place at $x = \ell/2$ with a voltage amplification lower than in the previous case;
- The zone with matched impedances $A \approx |Z_c|$ and $|B| < |Z_c|$ where resonance does not take place: the maximal voltage equals the input voltage $1V$ and there are discontinuities in the frequency and position surfaces.

The portion of the surface under the condition $|B| < |Zc|$ confirms the behavior described in [14]:

- for $|Z_L| < |Z_c|$ the resonance frequency is the same as for a short-circuited line
- for $|Z_L| > |Z_c|$ the resonance frequency is the same as for an open-ended line

However, the resonance frequency response shows that for loads with higher reactive components ($|B| > |Zc|$) this rule no longer applies. This is one of the main contribution of these surfaces: the resonance behavior of a cable can be assessed for any Z_L connected to the cable.

Table 2
Resonance behavior of the cable when connected to the example load Z_{L_e}.

Resonance frequency f_r	7.8 MHz
Voltage amplification $V(x_r)/V(0)$	5.8
Position of maximal voltage x_r	5 m

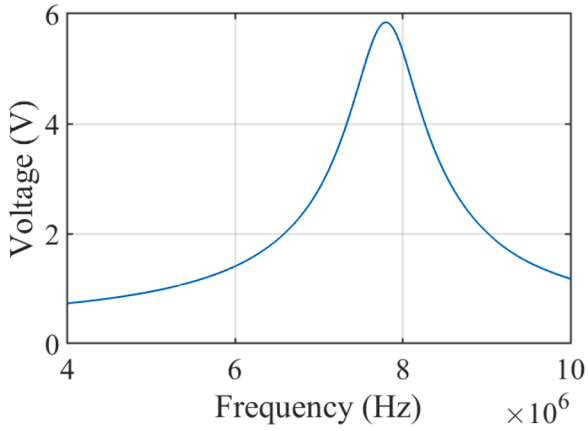

Fig. 7. Voltage at $x = 5\,m$ for the cable connected to the example load Z_e.

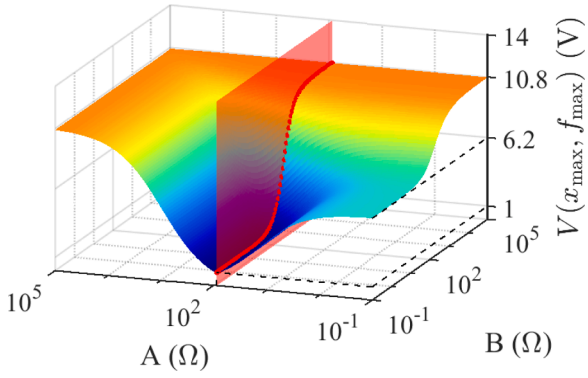

Fig. 8. Graphic visualization of the cuts from the resonance surface response. In this example, the cut from the intersection of the surface with the plane $A = Z_c$ is highlighted with red dots. (For interpretation of the references to color in this figure legend, the reader is referred to the web version of this article.)

Indeed, two distinct behaviors of the resonance were exposed by the surface:

- The maximum voltage occurs for a capacitive load to which the resonance frequency is lower than in the open-ended cable.
- The zone corresponding to inductive loads presents the only resonance taking place not at the midpoint, nor at the endpoint of the line, but varying in the interval $\ell/2 < x < \ell$.

These surfaces can be exploited as follows, using the example load Z_{L_e} presented in Fig. 6. Its input impedance was plotted in green in function of the frequency in Fig. 5c and d. The intersection between Z_{L_e} and the frequency surface gives the resonance frequency of the cable loaded by Z_{L_e}. The resonance voltage and position can then be assessed with the corresponding points in the remaining surfaces, points marked in pink in Fig. 5b and f. The resonance behavior of this example is resumed in Table 2.

In Fig. 7 the voltage at $x = 5\,m$ is plotted in function of the frequency, showing the peak of $5.8\,V$ at $f = 7.8\,MHz$. This simulation is also performed with the frequency-domain simulator validated in [12]).

Two original analysis are described in the following sections, to extend the applicability of the resonance surface response. Section 3.1 compares the resonance behavior of different two-conductor cables using 2D cuts from the 3D surfaces. Section 3.2 analyzes the impact of cable length in the resonance behavior.

3.1. Comparing cables using cuts from the resonance surface response

This section describes a method to compare the resonance behavior of different cables. One example of applicability of this method is the selection of power cables to be used in a system. Also, in this section the importance of taking the frequency-dependency of the cable parameters into account will be demonstrated.

Plotting several 3D surfaces in the same axis can make it difficult to visualize the data, and for this reason the comparison will be done with 2D cuts from the resonance surface response. A graphic representation of one of these 2D cuts is given in Fig. 8: it corresponds to the intersection between a plane and the resonance surface response.

The 2D cuts chosen for this analysis are the intersection between the surfaces and the planes $B = 0$, $A = 0$ and $A = |Z_c|$.

The cables to be compared are described in Table 3. The parameters of these cables were obtained with input impedance measurements, the parameters of the non-shielded cables can be found in [24] and the parameters of the coaxial cable are plotted in the Appendix.

A constant parameter example was added in this analysis to show the implications of using a simplified model of the cable when studying the resonance phenomenon in this frequency band. The values of the constant parameters were chosen to match the parameters of the two-conductor 0.75 mm^2 cable used in the previous section at the frequency $f = 1\,MHz$.

In this analysis the computation time can be drastically reduced by calculating the surface points exclusively for the values of (A, B) present in the 2D cuts. The cuts from the frequency and position surfaces could also be obtained, but they are omitted here for the sake of brevity.

The 2D cuts of the voltage surface are plotted in Fig. 9. The first cut in Fig. 9a corresponds to $B = 0$ and shows the resonance voltage when the cable is connected to a pure resistive load. From this curve the band around $|Z_c|$ where the behavior is close to impedance matching $Z_L = Z_c$ can be identified. Moreover, the open-circuit (OC) and short-circuit (SC) resonance voltages can be compared. The analysis with constant parameters overestimates the resonance amplification of the two-conductor 0.75 mm^2 cable for both OC and SC, because the losses at $1\,MHz$ are lower than at the resonance frequencies.

The second 2D cut $A = 0$ is plotted in Fig. 9b, and show the behavior of the resonance when the cable is connected to pure reactive loads. The peak of maximum voltage amplification is in the capacitive zone except for the coaxial cable that has its maximum voltage for an inductive load. As for the analysis with constant parameters, the maximum voltage amplification for a capacitive load visible for the $0,75\,mm^2$ is not present on the constant parameters cut, and the simplified model with constant p.u.l. parameters underestimates the maximum resonance-due voltage amplification.

The last cut corresponds to $A = |Z_c|$ and is plotted in Fig. 9c. In this figure the limit value of B that still allows the line to behave as a matched impedance line can be read. In all cases this limit is around $B < |Z_c|$.

These 2D cuts from the resonance surface response are those that best represent the overall shape of the 3D surfaces and are an efficient way to compare the resonance behavior of different cables.

This analysis demonstrates that if the cable model is simplified to constant p.u.l parameters the resonance-due voltage amplification can be dangerously underestimated, as it depends directly on the cable losses which vary drastically with the frequency. Also, because the p.u.l. inductance and capacitance vary with frequency [12], the resonance frequency can only be accurately determined if the model uses

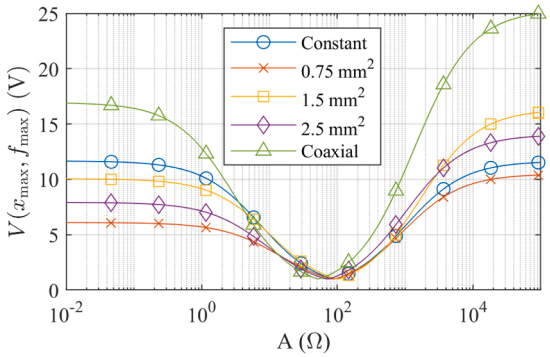

(a) $B = 0$, pure ressistive load

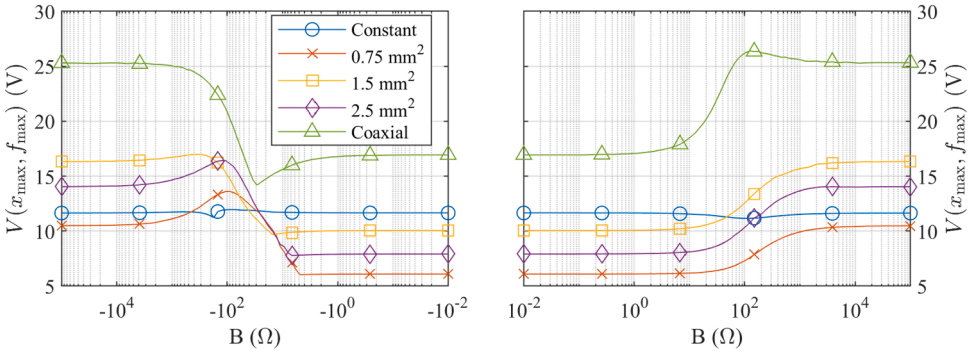

(b) $A = 0$, pure capacitive to the left, pure inductive to the right

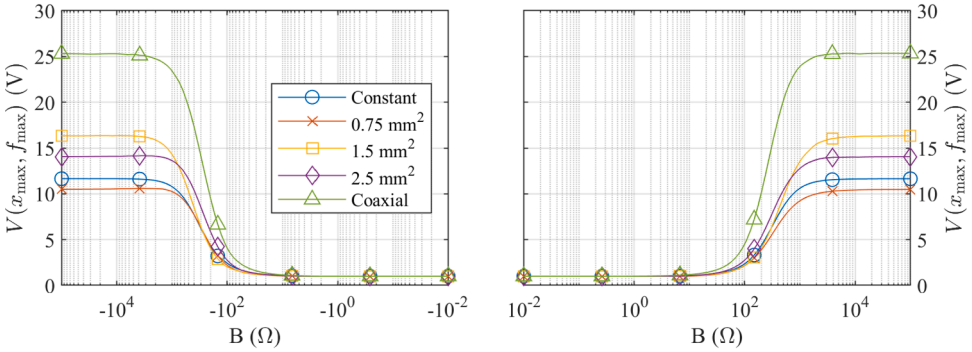

(c) $A = |Z_c|$, capacitive to the left, inductive to the right

Fig. 9. Cuts from the resonance surface responses of the cables described in Table 3.

Table 3
Description of the cables to be compared for their resonance behavior; R and G given for $f = 1$ MHz. The "constant parameters" are those of the 0.75 mm² cable at 1 *MHz*.

Cable	Application	$\lvert Z_c \rvert$ (Ω)	$R\left(\frac{\text{m}\Omega}{\text{m}}\right)$	$G\left(\frac{\mu S}{\text{m}}\right)$
Constant parameters	Example, $L = 578\,nH/m$ $C = 76,3$ pF/m	87	597.3	118.2
Two-conductor 0.75 mm²	Power cord	87.5	293.5	40.10
Two-conductor 1.5 mm²	Audio cable	105	347.0	12.43
Two-conductor 2.5 mm²	Power cord	71.8	251.9	25.19
Coaxial 50 Ω	RF signals	52.8	157.3	0.7610

frequency-dependent parameters.

As an example of analysis of the results in Fig. 9, suppose that a cable with a smooth resonance response is required. In that case, the two-conductor audio cable of section $1,5mm^2$ would be the best candidate. If the maximal resonance amplification of these cables is compared to their open-ended amplification in Fig. 9b, it is clear that the $1,5mm^2$ cable interacts less with reactive loads. This can be explained by the fact that this is an audio cable, designed to be robust against interference to maintain sound quality.

3.2. Analysis of the cable length impact on the resonance phenomenon

At first, the impact of the cable length on voltage amplification due to resonance may not be obvious. Indeed, the voltage amplification depends directly on the total losses in the cable given by the real component of $\mathbb{R}\{\gamma\ell\} = \alpha\ell$, were α is the attenuation coefficient, a direct representation of the cable losses.

The parameter α increases with frequency. The attenuation coefficient impacting the voltage amplification due to resonance is $\alpha(f_r)$, with

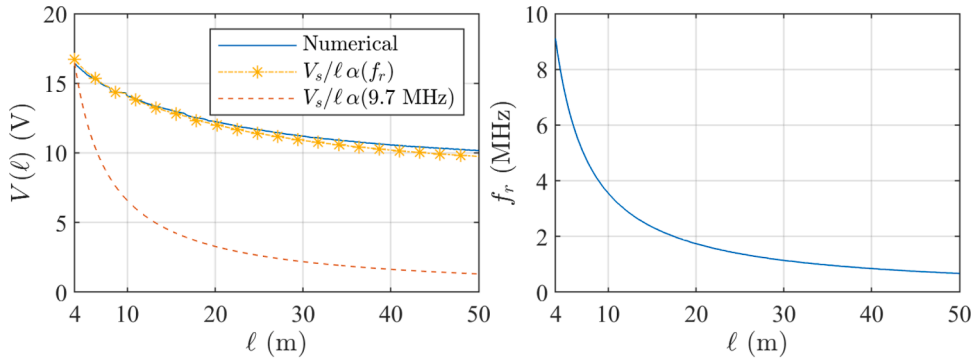

(a) $V(\ell)$ under resonance (b) f_r of the open-ended cable

Fig. 10. Analysis of the open-ended 2.5 mm^2 cable. In (a) $V(\ell)$ in function of cable length ℓ, the numerical solution (full line) is compared to (15) with both $\alpha(f_r)$ in asterisks and $\alpha(9.8\ \text{MHz})$ in the dashed line; the resonance frequency f_r is given in (b), and 9.8 MHz corresponds to f_r for $\ell = 4$ m.

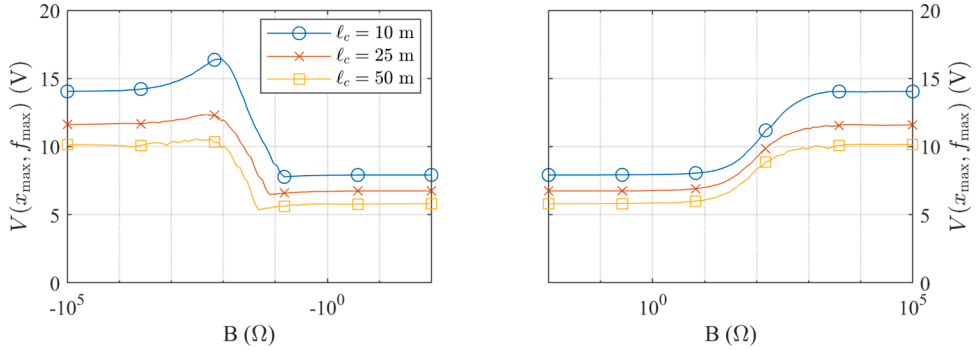

Fig. 11. Cut $A = 0$ of the resonance surface response of the 2.5 mm^2 cable for different cable lengths.

f_r the resonance frequency. Two characteristics must be considered:

- A longer cable will have higher total losses $(\alpha\ell)$ given a constant α, however;
- A longer cable will have a lower f_r, and therefore a lower $\alpha(f_r)$.

To study this aspect, a specific analysis of the voltage at $x = \ell$ of an open-ended cable was done. The resonance frequency of an open-ended cable is given by (12), what allows the approximation of $Z(0)$ for an open-ended cable at the resonance frequency f_r given in (13) [13]. The equation giving $V(\ell)$ is recalled in (14), what gives $V(\ell)^{OC}$ for $f = f_r$ as in (15).

$$f_r = \frac{v}{4\ell} \tag{12}$$

$$Z^{OC f=f_r} = Z_c \coth(\alpha\ell) \approx Z_c \alpha\ell \tag{13}$$

$$V(\ell) = V(0)\left[\cosh(\gamma\ell) + \frac{Z_c}{Z^{OC}}\sinh(\gamma\ell)\right] \tag{14}$$

$$V(\ell)^{OC f=f_r} = \frac{V_s}{\alpha\ell} \tag{15}$$

This approximation is validated in Fig. 10. In this figure, the method of the resonance surface response is used to extract the highest $V(\ell)$ from different excitation frequencies for a 2, 5 mm^2 cable with length varying from 4 m to 50 m. This numerical solution is then compared to the same voltage calculated from Eq. (15), first using the attenuation coefficient corresponding to the resonance frequency f_r given by (12) and secondly using α for 9.8 *MHz*, corresponding to the resonance frequency of a 4 m long cable.

Figure 10 shows that the factor $\ell\,\alpha(f_r)$ increases with the cable length despite the reduction of the resonance frequency, attenuating the resonance voltage. Still, this attenuation would be greater if the cable losses were constant (dashed line).

To generalize this analysis, the resonance surface response is again necessary. They were calculated for three different lengths of the 2, 5 mm^2 cable and for most of the regions of the surface the voltage amplification was reduced by a constant factor as length increases, except for pure reactive loads.

For this reason the cut $A = 0$ is the only one presented here in Fig. 11. It shows that, other than the fact that the voltage amplification reduces with cable length, the resonance voltage peak for capacitive loads around $B = -10^2\ \Omega$ is attenuated as the cable length increases.

In conclusion, longer power cables tend to have lower harmonic amplifications, even if the losses impacting the resonance tend to reduce.

4. Higher-dimensional resonance surface response

The three-dimension resonance surface response presented in the previous section applies exclusively to systems that can be represented with a two-conductor transmission line model. If the circulation of parasitic currents is considered the two-conductor cable model is not sufficient to represent the system.

Therefore, to expand the applicability of the resonance surface approach the multiconductor TL model must be studied and the resonance surface defined for higher dimensions. This is another original contribution of this work.

A generic model has to consider a $(n+1)$-conductor cable, with n active conductors and one reference conductor. This cable would have its terminals connected to $(n+1)$-port Thévénin/Norton equivalent circuits, as shown in Fig. 2. For these equivalent circuits to be generic, they would require at least $(n+1)n/2$ impedances to be identified [23].

As the resonance surface response needs an axis to represent each of the real and the imaginary part of the impedances composing $\mathbf{Z_S}$ and $\mathbf{Z_L}$, plus one axis to represent the result variable (maximal voltage/current, frequency, position) the resonance surface response should have $2(n+1)$ $n+1$ dimensions for a $(n+1)$-conductor cable in its most generic representation.

The generic system can be simplified to a source-cable-load schematics by canceling impedance matrix $\mathbf{Z_S}$ and source vector $\mathbf{I_L}$. In this case $(n+1)n+1$ dimensions would be needed for a $(n+1)$-conductor cable, and the surface cannot be visualized for $n>1$.

The decomposition of a system with a $(n+1)$-conductor cable into n modal two-conductor systems is possible according to the theory described in [25,26]. The decomposition proposed in these works is based on the diagonalization of p.u.l. parameter matrices **YZ** and **ZY** with a decomposition matrix **T**.

However, in power cables these parameters vary considerably with frequency, and in the general case different **T** are needed for different frequencies. A 3D resonance surface response derived from a frequency-dependent decomposition would have no meaning at all: modal voltages on different basis cannot be compared.

Moreover, for the whole system to be decomposed **T** should also diagonalize $\mathbf{Z_L}$, what is not guaranteed in the most general case.

That leaves two options of analysis, depending on the system characteristics:

- A single frequency independent transformation allows the decomposition of the $n+1$-conductors cable model, the source and load equivalent circuits into n two-conductor modal subsystems, and the resonance frequency response can be plotted in 3D for each mode.
- Such a transformation is not possible, and the resonance frequency response will be in higher dimensions. Even though it cannot be plotted, an optimization algorithm can be used to analyze it.

These two possibilities are studied in the next two subsections, respectively.

4.1. Frequency independent decomposition of systems with multiconductor cables

As aforementioned, to represent systems with multiconductor cables with 3D resonance surfaces a single frequency independent **T** able to diagonalize all the matrices modeling the system (**YZ**, **ZY**, $\mathbf{Z_L}$ and $\mathbf{Z_S}$, cf. Fig. 2) is needed. There are special cases where this is possible.

A first example is a three-conductor balanced system, i.e. a system with decoupled common mode (CM) and differential mode (DM), assuming that the third conductor is the common-mode path, e.g. cable shield or earth return. The CM/DM decomposition is given by Eqs. (16) and (17).

$$V_{DM} = V_1 - V_2 \qquad I_{DM} = \frac{I_1 - I_2}{2} \tag{16}$$

$$V_{CM} = \frac{V_1 + V_2}{2} \qquad I_{CM} = I_1 + I_2 \tag{17}$$

In a balanced system all elements source, cable and load are balanced [27]. A cable is balanced if it is cyclic symmetric [22], i.e. the cross-section of the cable has the same geometry when rotated by a symmetry angle θ.

These observations lead to the generalization of this example: a frequency independent modal decomposition of a $n+1$-conductor system is possible if the cable, the load and the source are cyclic symmetric. If that is the case, the parameters matrices **Z** and **Y** and terminal matrices $\mathbf{Z_L}$ and $\mathbf{Z_S}$ are circulant [28], and a possible orthonormal decoupling matrix **T** is given by (18) (see [22] on page 300 for more details)

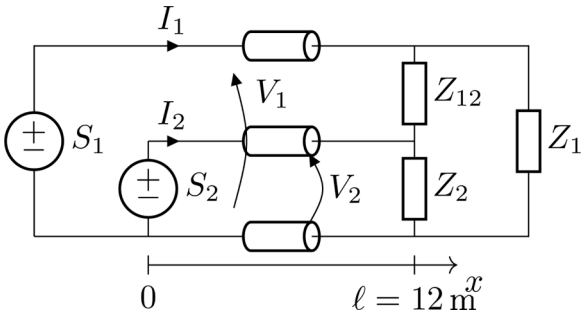

Fig. 12. Schematics of a generic model for a three-conductor cable system, voltage sources $S_1 = 1,5\,V$ and $S_2 = 0,5\,V$ with variable frequency, cable length $\ell = 10\,m$. The resonance analysis is performed in function of the load impedances Z_1, Z_{12}, Z_2.

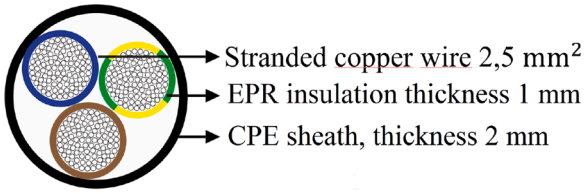

Fig. 13. $2.5\,\mathrm{mm}^2$ three-conductor cable cross-section.

$$[\mathbf{T}]_{ij} = \frac{1}{\sqrt{n}} \exp\left[\frac{2\pi}{n}(i-1)(j-1)\right] \tag{18}$$

It is true that many power cables are cyclic symmetric, but cyclic symmetric devices (loads) with $n>2$ are less common. One rare example is three-phase electrical machines.

An example of 3D resonance surface response for a three-conductor balanced system using the differential/common-mode decomposition can be found in a previous work by the same authors [17]. The systems that do not present cyclic symmetry can only be analyzed by the general approach described in the next section.

4.2. Seven-dimensional surface

Higher dimensional surfaces are needed to describe a generic system with multi-conductor cables. Here the resonance surface response of a three-conductor cable will be studied, taking the hypothesis that all currents circulate exclusively through these three conductors (no earth return).

In this example, the generic schematic presented in Fig. 2 was simplified to the system in Fig. 12. The resonance surface response will be computed in function of the maximum between $V_1(x)$ and $V_2(x)$. The simulations are performed with the frequency-domain simulator described and validated experimentally in [12].

The resonance surface response of the cable in Fig. 12 requires one axis for each the real and imaginary parts of the three load impedances, plus one axis for the resonance voltage, frequency or position. Therefore, seven dimensions are needed to describe the surface (as stated before: $(n+1)n+1$ with $n=2$).

This surface cannot be plotted, but an optimization algorithm will be used to investigate it. Thus, the surface is not entirely calculated, instead the optimization algorithm chooses the points to be evaluated on its search for a maximum in the voltage surface.

For this example the parameters from a three-conductor cable of section $2.5\,\mathrm{mm}^2$ are used. A cross-section of the cable is presented in Fig. 13. This cable is commonly used for power cords of single-phase devices needing a protective earth (PE) conductor. The parameters of the cable were identified with input impedance measurements and are given in Fig. 3.19 of [24].

Table 4
Scaling of variables and goal function domain of the resonance surface response optimization with the sequential quadratic programming (SQP) algorithm, with soft constraints. Cable length $\ell = 10\,m$, open circuit for $Z = 1\,M\Omega$.

Variable	Scale	Range
f	linear	[1,10] MHz
x	linear	$[0, \ell]$ m
A_1, A_{12}, A_2	log	$[0] \cup [10^{-2}, 10^{6}]\,\Omega$
B_1, B_{12}, B_2	log	$[-10^{6}, -10^{-2}] \cup [0] \cup [10^{-2}, 10^{6}]\,\Omega$

The amplitude of the sources feeding the cable are set to $S_1 = 1.5$ V and $S_2 = 0.5$ V, so that the equivalent sources in differential and common mode have both an amplitude of 1 V (see Eqs. (16) and (17)).

The optimization algorithm will minimize the goal function (19). The points of minima of this function correspond to the points of maxima between the two voltages $V_1(x,f)$ and $V_2(x,f)$, and the exp function serves to expand the function around these points.

$$F(X) = -\exp[\max[V_1(x,f), V_2(x,f)]] \tag{19}$$

In this study, an initial analysis was performed to investigate the general behavior of the surface identifying multiple local maxima for different load impedances; it is described in Section 4.2.1. To refine the results, a second analysis with additional constraints based on a real system was performed, resulting in one single point of maximum voltage; this is described in Section 4.2.2.

4.2.1. *Soft-constrained optimization*

In the first stage of this analysis a loosely constrained optimization is performed with a deterministic algorithm, (sequential quadratic programming - SQP) [29] in the domain described in Table 4.

The maximum value of the impedances is defined as $1\,M\Omega$, what will be considered an open circuit from here on.

The optimization results on different maxima for different initial points, meaning that the surface has multiple local maxima. These points can give an intuition of how the surface behaves and for that reason a systematic method was established to obtain as many local maxima as possible.

The deterministic optimization was performed for 50 random initial points generated from a Sobol sequence that fills the space uniformly [30]. Six different points of local maxima were identified with this method and labeled "a" to "f". They are graphically represented using numeric rulers in Fig. 14.

Figure 14 can be read as follows: for the maximum point labeled "f", the first ruler gives its voltage amplification ($V_{max} \approx 25.3V$). The second ruler gives the frequency to which the amplification took place ($f_n \approx 3.75\,MHz$). The six following rulers represent the terminal impedance that lead to this resonance point: $B_1 = B_2 = B_{12} = 1\,M\Omega$, what corresponds to an open-circuit.

It cannot be guaranteed that these are all the local maxima. Still, it is interesting to note that a very similar voltage amplification can be obtained with a different combination of impedance loads, as shown by the points labeled "a", "c", "d" and "e" practically superposed in the V_{max} ruler.

However, in a practical application the optimization constraints would be stronger and it is possible to find a unique solution. This is discussed in the next subsection.

4.2.2. *Strongly constrained optimization*

In the second stage of this study, the constraints of the optimization problem were modified to adapt to a more realistic scenario, as follows: conductor 2 is the phase conductor, conductor 1 is the neutral conductor and conductor 0 is the protective earth (PE).

In this scenario the impedances Z_1 and Z_2 represent parasitic capacitances between the circuitry and the chassis, i.e. common-mode capacitances, and Z_{12} represents the device input impedance, i.e. the differential-mode impedance.

These definitions allow the inclusion of new constraints in the optimization. Taking the hypothesis that differential-mode input impedance will not assume higher values than 1 kΩ, and that the common-mode capacitances will not be greater than 100 pF; these are common values for a single-phase load. The optimization constrains can be defined as presented in Table 5.

The constrained optimization was performed with a genetic algorithm (GA) coupled with a deterministic algorithm (SQP). With the parameters given in Table 5, the optimization finds a single voltage maximum systematically, given in Table 6.

The characteristics of the point labeled "a" of Fig. 14 are also listed in Table 6 for comparison, because it is the closest point to the optimum from the previous analysis. However, the point "a" would be outside the domain of this constrained problem (cf. Table 5).

The resonance configuration given in Table 6 occurs if the cable is connected to the load in Fig. 15a. With the frequency-domain simulator validated in [12] the voltages at $x = \ell$ are calculated for this specific load, and the result is plotted in Fig. 15b. The maximal voltage $V(\ell)$ occurs for the frequency predicted by the resonance surface response $f_r = 3.27$ MHz, and with the same amplification of 27.12 V.

Table 5
Extra constraints for the second stage of the study, optimization run with genetic algorithm (GA) [31] followed by a sequential quadratic programming (SQP) algorithm.

Diff. mode	$\lvert Z_{12}\rvert < 1\,\text{k}\Omega$
Common mode	$Z_1, Z_2 = -jB, \quad B \in \left[\frac{1}{2\pi f 100\,\text{pF}}, 1\,\text{M}\Omega\right]$

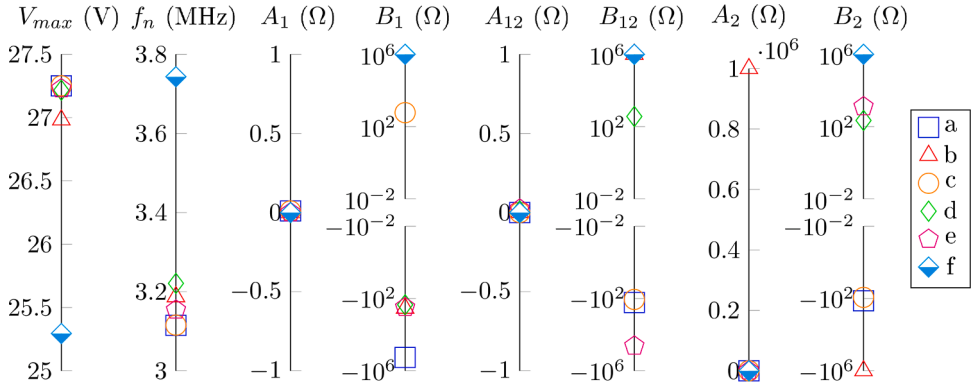

Fig. 14. Light-constrained optimization results, six local maxima plotted in the 8 numeric rulers. Each ruler represents one axis of the higher dimensional space, and the coordinates of each point of maximum are plotted over these axes. All maxima occurred for $x = \ell = 10\,m$.

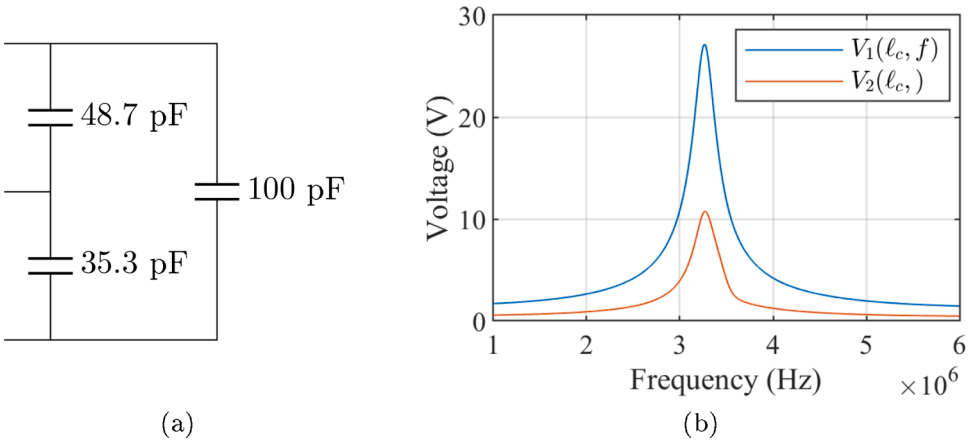

Fig. 15. (a): equivalent load of the maximum voltage amplification point in Table 6, and (b): corresponding simulation of the voltages at $x = \ell$.

Table 6
Comparison of the constrained optimization result with the closest local maxima from Fig. 14.

	Constrained optimization	Label "a" of Fig. 14
V_{max}	27.12 V	27.25 V
f_{max}	3.27 MHz	3.11 MHz
Z_1	$-j487.4\ \Omega$	$-j183.3\ k\Omega$
Z_{12}	$-j1\ k\Omega$	$-j167.5\ \Omega$
Z_2	$-j1.381\ k\Omega$	$-j134.0\ \Omega$

It is unlikely that a real single-phase device would have the input impedance given in Fig. 15a, seen that the common-mode impedance Z_{12} is a capacitance of lower value than the parasitic capacitance in Z_{11}. This indicates that the chosen constraints in Table 5 are still more loose than desired. However, in a real case application these constraints could be more easily defined and the results would be more realistic.

Note that the critical load in Fig. 15a is unbalanced, therefore it could not be found with an analysis based on a common, differential-mode decomposition as discussed in Section 4.1 and detailed in [17]. Only the analysis of higher dimension surfaces proposed here is able to find this point of maximum in the resonance-due voltage amplification.

The higher-dimension resonance surface response presented in firsthand here is able to characterize the resonance behavior of a generic system, and when coupled with an optimization algorithm it can contribute to the design of robust systems against resonance phenomenon.

5. Conclusion

The resonance surface response method proposed in this paper is a contribution to the modeling and analysis of the resonance phenomenon in long multiconductor cables. It is well adapted to take the frequency-dependent cable parameters into account, and can be applied as long as the devices connected to its terminals can be linearized. There is no need for these devices to be balanced, or symmetric in any other way. The analysis of resonance with such a generic model is an original contribution to the literature. The resonance surface response can be visualized if it is contained in three dimensions, i.e. when it is calculated in function of two scalar variables. The first example of resonance in this paper was plotted in function of the real and imaginary parts of a load impedance, but other variables can be chosen, e.g. the reactive elements of a filter. The three-dimension surface was useful to show that taking the hypothesis of constant cable parameters can induce to serious errors in the prediction of the worst-case resonance, both for the resonance frequency and amplitude. Also, an original analysis of the resonance in function of the cable length shows that for the power cable under study the increase of the cable length does reduce the resonance amplitude, but at a much slower rate than a constant-parameter model would have predicted. If the surfaces are needed in function of more than two scalar variables, the surface will be defined on higher dimensions and an optimization algorithm is necessary to analyze it. The example given in this work shows how to proceed to analyze an unbalanced system, a subject presently in demand in the literature. One of the interesting perspectives arising from this analysis is the design of EMI filters for such systems. Indeed, the method is well adapted to design EMI preventive measures where the whole systems is known to the developers, e.g. distributed power plants and electric vehicles. In such cases the proposed method can predict accurately the maximal conducted emissions in the system, information that can allow the design of robust EMI filters, contribute to the choice of the cable insulation level, etc. The authors identified two drawbacks of the proposed method : the potential computational effort, and the need of a linear frequency-domain model of power converters if they are connected to the cable. The frequency-domain simulator used to compute the surfaces is efficient, and when coupled with an optimization algorithm the computational effort required for the resonance surface approach is acceptable. As for the linearization of the power converters, there are multiple references in the literature with efficient linear models for such devices. In conclusion, the proposed method gives interesting perspectives of designing robust systems against the resonance-due amplification of EMI emissions.

CRediT authorship contribution statement

Tamiris G. Bade: Conceptualization, Methodology, Software, Validation, Writing – original draft. **James Roudet:** Project administration, Conceptualization, Writing – review & editing. **Jean-Michel Guichon:** Conceptualization, Writing – review & editing. **Patrick Kuo-Peng:** Supervision, Writing – review & editing. **Carlos A.F. Sartori:** Supervision, Writing – review & editing.

Declaration of Competing Interest

We wish to draw the attention of the Editor to the following facts which may be considered as potential conflicts of interest and to significant financial contributions to this work. We wish to confirm that there are no known conflicts of interest associated with this publication and there has been no significant financial support for this work that could have influenced its outcome. We confirm that the manuscript has been read and approved by all named authors and that there are no other persons who satisfied the criteria for authorship but are not listed. We further confirm that the order of authors listed in the manuscript has

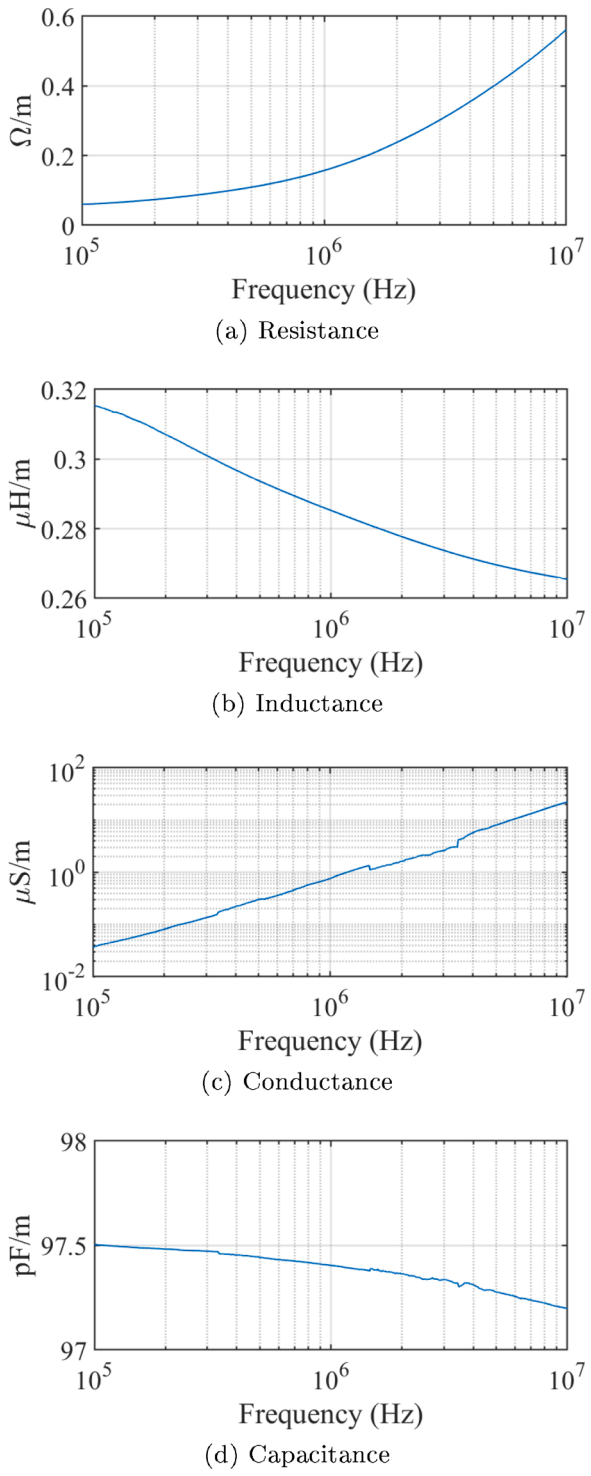

Fig. 16. Per-unit-length parameters of the coaxial cable introduced in Section 3.

been approved by all of us. We confirm that we have given due consideration to the protection of intellectual property associated with this work and that there are no impediments to publication, including the timing of publication, with respect to intellectual property. In so doing we confirm that we have followed the regulations of our institutions concerning intellectual property. We understand that the Corresponding Author is the sole contact for the Editorial process (including Editorial Manager and direct communications with the office).She is responsible for communicating with the other authors about progress, submissions of revisions and final approval of proofs. We confirm that we have provided a current, correct email address which is accessible by the Corresponding Author.

Appendix A. Appendix A

The parameters of the coaxial cable obtained with an identification based on the input impedance measurement [12] are plotted in Fig. 16.

References

[1] M. Cirrincione, M. Pucci, G. Vitale, Direct power control of three-phase VSIs for the minimization of common-mode emissions in distributed generation systems, Electr. Power Syst. Res. (2011), https://doi.org/10.1016/j.epsr.2010.11.007.
[2] R.J. Kerkman, D. Leggate, G.L. Skibinski, Interaction of drive modulation and cable parameters on AC motor transients, IEEE Trans. Ind. Appl. (1997), https://doi.org/10.1109/28.585863.
[3] Marios C. Sousounis,, Jonathan K. H. Shek,, Markus A. Mueller, Filter design for cable overvoltage and power loss minimization in a tidal energy system with onshore converters, IEEE Trans. Sustain. Energy (2016), https://doi.org/10.1109/TSTE.2015.2424258.
[4] S. Zhang, S. Jiang, X. Lu, B. Ge, F.Z. Peng, Resonance issues and damping techniques for grid-connected inverters with long transmission cable, IEEE Trans. Power Electron. (2014), https://doi.org/10.1109/TPEL.2013.2253127.
[5] S. Liu, F. Lin, X. Fang, Z. Yang, Z. Zhang, Train impedance reshaping method for suppressing harmonic resonance caused by various harmonic sources in trains-network systems with auxiliary converter of electrical locomotive, IEEE Access (2019), https://doi.org/10.1109/ACCESS.2019.2958880.
[6] L. Zhai, X. Zhang, N. Bondarenko, D. Loken, T.P. Van Doren, D.G. Beetner, Mitigation emission strategy based on resonances from a power inverter system in electric vehicles, Energies (2016), https://doi.org/10.3390/en9060419.
[7] D. Drozhzhin, G. Griepentrog, A. Sauer, R.D. Maglie, A. Engler, Investigation on differential to common mode coupling in the output cable of AC drive for more electric aircraft. 2017 19th European Conference on Power Electronics and Applications (EPE'17 ECCE Europe), 2017, https://doi.org/10.23919/EPE17ECCEEurope.2017.8098927.
[8] H. Akagi, I. Matsumura, Overvoltage mitigation of inverter-driven motors with long cables of different lengths, IEEE Trans. Ind. Appl. (2011), https://doi.org/10.1109/TIA.2011.2154294.
[9] H.D. Paula, D.A.d. Andrade, M.L.R. Chaves, J.L. Domingos, M.A.A.d. Freitas, Methodology for cable modeling and simulation for high-frequency phenomena studies in PWM motor drives, IEEE Trans. Power Electron. (2008), https://doi.org/10.1109/TPEL.2007.915759.
[10] L. Wang, C.N.-M. Ho, F. Canales, J. Jatskevich, High-frequency modeling of the long-cable-fed induction motor drive system using TLM approach for predicting overvoltage transients, IEEE Trans. Power Electron. (2010), https://doi.org/10.1109/TPEL.2010.2047027.
[11] D. de Paula dos Santos, C.A.F. Sartori, Impact of mismatch cables impedances on active motor terminal overvoltage mitigation using parallel voltage source inverters. 2017 IEEE 3rd Global Electromagnetic Compatibility Conference (GEMCCON), 2017, https://doi.org/10.1109/GEMCCON.2017.8400662.
[12] T.G. Bade, J. Roudet, J.-M. Guichon, P. Kuo-Peng, C.A. Sartori, Frequency-domain modeling of unshielded multiconductor power cables for periodic excitation with new experimental protocol for wide band parameter identification, Electr. Eng. (2019), https://doi.org/10.1007/s00202-019-00780-2.
[13] W.C. Johnson, Transmission Lines and Networks, McGraw-Hill, 1950.
[14] A.I. Chrysochos, T.A. Papadopoulos, G.K. Papagiannis, Rigorous calculation method for resonance frequencies in transmission line responses, IET Gener. Transm. Distrib. (2014), https://doi.org/10.1049/iet-gtd.2014.0948.
[15] A. Pană, A. Băloi, F. Molnar-Matei, A numerical analysis of the harmonic impedance in a medium voltage AC network. 8th International Conference on Modern Power Systems (MPS), 2019, https://doi.org/10.1109/MPS.2019.8759741.
[16] D. Darmawardana, S. Perera, J. Meyer, D. Robinson, U. Jayatunga, S. Elphick, Development of high frequency (Supraharmonic) models of small-scale (<5kw), single-phase, grid-tied PV inverters based on laboratory experiments, Electr. Power Syst. Res. (2019), https://doi.org/10.1016/j.epsr.2019.105990.
[17] T.G. Bade, J. Roudet, J.-M. Guichon, P. Kuo-Peng, C.A. Sartori, Robust filter design technique to limit resonance in long cables connected to power converters, IEEE Trans. EMC (2020), https://doi.org/10.1109/TEMC.2020.2993082.
[18] B. Revol, J. Roudet, J. Schanen, P. Loizelet, EMI study of three-phase inverter-fed motor drives, IEEE Trans. Ind. Appl. (2011), https://doi.org/10.1109/TIA.2010.2091193.
[19] Z. Chen, A. Luo, H. Kuang, L. Zhou, Y. Chen, Y. Huang, Harmonic resonance characteristics of large-scale distributed power plant in wideband frequency domain, Electr. Power Syst. Res. (2017), https://doi.org/10.1016/j.epsr.2016.09.001.
[20] C.F. Jensen, Harmonic background amplification in long asymmetrical high voltage cable systems, Electr. Power Syst. Res. (2018), https://doi.org/10.1016/j.epsr.2018.03.009.
[21] I. Sowa, J.L. Domínguez-García, O. Gomis-Bellmunt, Impedance-based analysis of harmonic resonances in HVDC connected offshore wind power plants, Electr. Power Syst. Res. (2019), https://doi.org/10.1016/j.epsr.2018.10.003.

[22] C. Paul, Analysis of Multiconductor Transmission Lines, IEEE Press, 2008.
[23] M. Hosoya, The simplest equivalent circuit of a multi-terminal network, 2000.
[24] BadeT. G.. Characterization of the cabling on industrial power networks for EMI simulation, Communauté UGA, 2019. Phd thesis.
[25] G.G. Gentili, M. Salazar-Palma, The definition and computation of modal characteristic impedance in quasi-TEM coupled transmission lines, IEEE Trans. Microwave Theory Tech. (1995), https://doi.org/10.1109/22.348093.
[26] C.R. Paul, Decoupling the multiconductor transmission line equations, IEEE Trans. Microwave Theory Tech. (1996), https://doi.org/10.1109/22.536026.
[27] A. Sugiura, Y. Kami, Generation and propagation of common-mode currents in a balanced two-conductor line, IEEE Trans. EMC. (2012), https://doi.org/10.1109/TEMC.2011.2162523.
[28] C.Y. Chao, Circulant matrices (Philip J. Davis), SIAM Rev. (1982), https://doi.org/10.1137/1024081.
[29] R. Fletcher, The Sequential Quadratic Programming Method, Springer Berlin Heidelberg, pp. 165–214. 10.1007/978-3-642-11339-0_3.
[30] S. Joe, F.Y. Kuo, Remark on algorithm 659: Implementing Sobol's quasirandom sequence generator, ACM Trans. Math. Softw. (TOMS) (2003), https://doi.org/10.1145/641876.
[31] K. Deb, Introduction to Genetic Algorithms for Engineering Optimization, Springer Berlin Heidelberg, pp. 13–51. 10.1007/978-3-540-39930-8_2.